THE JOURNAL OF BIOLOGICAL CHEMISTRY
Vol. 280, No. 19, Issue of May 13, pp. 19177–19184, 2005
Printed in U.S.A.

Substrate Binding Stoichiometry and Kinetics of the Norepinephrine Transporter*

Received for publication, November 15, 2004, and in revised form, March 7, 2005
Published, JBC Papers in Press, March 9, 2005, DOI 10.1074/jbc.M412923200

Joel W. Schwartz‡, Gaia Novarino§, David W. Piston¶, and Louis J. DeFelice‡‖**

From the ‡Center for Molecular Neuroscience, Departments of ‖Pharmacology and ¶Molecular Physiology and Biophysics, Vanderbilt University Medical Center, Nashville, Tennessee 37232-8548 and the §Dipartimento di Biologia Cellulare e dello Sviluppo, Università Roma 1 "La Sapienza," P.le Aldo Moro 5, 00185 Roma, Italy

The human norepinephrine (NE) transporter (hNET) attenuates neuronal signaling by rapid NE clearance from the synaptic cleft, and NET is a target for cocaine and amphetamines as well as therapeutics for depression, obsessive-compulsive disorder, and post-traumatic stress disorder. In spite of its central importance in the nervous system, little is known about how NET substrates, such as NE, 1-methyl-4-tetrahydropyridinium (MPP^+), or amphetamine, interact with NET at the molecular level. Nor do we understand the mechanisms behind the transport rate. Previously we introduced a fluorescent substrate similar to MPP^+, which allowed separate and simultaneous binding and transport measurement (Schwartz, J. W., Blakely, R. D., and DeFelice, L. J. (2003) *J. Biol. Chem.* 278, 9768–9777). Here we use this substrate, 4-(4-(dimethylamino)styrl)-*N*-methyl-pyridinium (ASP^+), in combination with green fluorescent protein-tagged hNETs to measure substrate-transporter stoichiometry and substrate binding kinetics. Calibrated confocal microscopy and fluorescence correlation spectroscopy reveal that hNETs, which are homomultimers, bind one substrate molecule per transporter subunit. Substrate residence at the transporter, obtained from rapid on-off kinetics revealed in fluorescence correlation spectroscopy, is 526 μs. Substrate residence obtained by infinite dilution is 1000 times slower. This novel examination of substrate-transporter kinetics indicates that a single ASP^+ molecule binds and unbinds thousands of times before being transported or ultimately dissociated from hNET. Calibrated fluorescent images combined with mass spectroscopy give a transport rate of 0.06 ASP^+/hNET-protein/s, thus 36,000 on-off binding events (and 36 actual departures) occur for one transport event. Therefore binding has a low probability of resulting in transport. We interpret these data to mean that inefficient binding could contribute to slow transport rates.

Adrenergic signaling in the central nervous system modulates learning and memory, the fight-or-flight response, and the reception of pain (2). Noradrenaline (norepinephrine, NE)[1] is the principal transmitter in postganglionic sympathetic neurons (3), and in the brainstem NE regulates autonomic function (4). Noradrenergic dysfunction is associated with mood disorders and depression (5, 6), post-traumatic stress disorder (7), hypertension, diabetes, cardiomyopathy, and heart failure (8). After stimulated or spontaneous NE release, NETs rapidly clear NE from the synaptic cleft via efficient transport system attenuating signaling (9), and recycling 90% of synaptic NE (10). A polymorphism in hNET causing decreased uptake correlates with orthostatic intolerance (11–13). hNETs are targets for cocaine, antidepressants, amphetamines, and neurotoxins (14, 15). Drugs that block NETs or replace NE anomalously increase NE levels and prolong signaling. In particular, the neurotoxin 1-methyl-4-tetrahydropyridinium (MPP^+), an monoamine oxidase (MAO-B) metabolite of 1-methyl-4-phenyl-1,2,5,6-tetrahydropyridine, inhibits mitochondrial respiration and induces Parkinson disease symptoms (16). Understanding hNET and how substrates and drugs interact with this transporter are fundamental questions in neuroscience.

The mechanism of NE transport and drug interfere are only partially understood, one obstacle being few data on substrate-transporter interactions. NET belongs to a gene family that uses the Na^+ gradient to transport transmitters (14). Hydropathy plots and antibody accessibility data imply that NETs have 12 transmembrane domains with intracellular N and C termini and a large extracellular loop between transmembrane domains II and III (14, 17). A single gene encodes hNET (18); however, biochemical evidence predicts that NETs are multimers (19). Furthermore, related transporters for serotonin (SERT) and dopamine (DAT) function as multimers (20, 21), also suggested by fluorescence resonance energy transfer (22) and cross-linking experiments (23). Directional cross-linking and Zn^{2+} binding suggest that DAT consists of homodimers (24–26), and Kocabas *et al.* (19) measured oligomerization by co-immunoprecipitation of tagged NETs. Thus, monoamine transporters function as homomultimers (27), but the number of bound substrates per functional unit is unknown.

In vitro studies in tissue culture, resealed membrane vesicles, cultured cells, and synaptosomes demonstrate that NE accumulation saturates at micromolar concentrations, but Na^+ and Cl^- dependence saturate in the millimolar range (28). The accepted mechanism for co-transporters is the fixed stoichiometry, alternating access model (29), which predicts NET transports 1NE:1Na:1Cl roughly once per second (30, 31); however, NET-

* This work was supported by National Institutes of Health NS-34075 and DA-6338 (to L. J. D.), CA68485 and DK20593 (to D. W. P.), and MH 58921 (to J. W. S.). The costs of publication of this article were defrayed in part by the payment of page charges. This article must therefore be hereby marked "*advertisement*" in accordance with 18 U.S.C. Section 1734 solely to indicate this fact.

** To whom correspondence should be addressed: Dept. of Pharmacology, Vanderbilt University Medical Center, Nashville, TN 37232-8548. Tel.: 615-343-6278; Fax: 615-343-1679; E-mail: lou.defelice@vanderbilt.edu.

[1] The abbreviations used are: NE, norepinephrine; hNET, human norepinephrine transporter; MPP^+, 1-methyl-4-tetrahydropyridinium; FCS, fluorescence correlation spectroscopy; FLIM, fluorescence lifetime imaging microscopy; TIRF, total internal reflection fluorescence; DS, desipramine; DiO, 3,3′-dioctadecyloxacarbocyanine perchlorate; GFP, green fluorescent protein; FRAP, fluorescence recovery after photobleach; KRH, Krebs-Ringer-Hepes.

mediated currents are 100 times larger than predicted by this model (32). Similar currents exist in native cells (33–38), and the charge-to-substrate ratio is an important key to mechanism (39).

Here we use fluorescence methodology and patch clamp to compare ASP^+ binding, ASP^+ transport, and ASP^+-induced current. After adding ASP^+, hNET-expressing cells intensify fluorescence initially to binding and secondarily to transport (1). Here we use morphological markers to distinguish plasma membrane-localized ASP^+ (bound to the cell surface) from mitochondrial ASP^+ (transported into the cell). Using fluorescence lifetime imaging microscopy (FLIM), total internal reflection fluorescence (TIRF) microscopy, and fluorescence correlation microscopy (FCS) with ASP^+ and GFP-tagged hNETs, we directly measure substrate-transporter kinetics, substrate-transporter stoichiometry, transporter, and substrate surface density, transport rates, and charge/substrate ratios. These data provide a novel model of neurotransmitter co-transport, in which the rate-limiting step is not exclusively large conformation changes but also inefficient binding, expressed as the low probability of transport following binding.

MATERIALS AND METHODS

Reagents—Experiments were at room temperature unless noted. ASP^+ and DiO were from Molecular Probes (Eugene, OR), soluble recombinant EGFP from Clontech (Palo Alto, CA), and other chemicals from Sigma. Images were processed with MetaMorph software (Universal Imaging Corp., Downington, PA). P. Bissel at Virginia Polytechnic synthesized deuterated ASP^+. Methyliodide-*d*3 (84 ml, 1.4 mmol) was added to *trans*-4-[4-(dimethylamino)-styryl]pyridine (100 mg, 0.45 mmol) in *N*,*N*-dimethylformamide (2 ml), and added at 4 h to 20 ml of ether and filtered. The crude product crystallized from methanol gave pyridinium salt as purple needles (111 mg, 67%, m.p. 256 °C), validated by ^1H NMR and ^{13}C NMR.

Cell Culture—HEK293 cells were kept in Dulbecco's modified Eagle's medium with 10% fetal bovine serum (v/v), 2 mM glutamine, 100 IU/ml penicillin, and 100 μg/ml streptomycin (Invitrogen). Stable lines expressing hNET (hNET-293) are previously described (32, 40). N-terminal GFP-tagged hNET cDNA was a gift from S. Amara. Stable GFP-tagged hNET (GFP-hNET) cells (GFP-hNET-293) were generated by G418 antibiotic selection. HEK293 were FuGENE 6 transfected with GFP-hNET-293 cDNA. At 24 h, transfected cells were selected (G418 250 μg/ml) and colonies were examined for ASP^+ or NE uptake. Stable lines were maintained under G418 selection.

Radiometric and Mass Spectrometric Transport Assay—hNET-293 cells were plated on poly-L-lysine-coated 24-well plates, 10^5 cells per well, 3 days before transport assays (90% confluence on 3rd day, media removed by aspiration). Cells were preincubated 10 min in Krebs-Ringer-Hepes (KRH, mM: 130 NaCl, 1.3 KCl, 2.2 $CaCl_2$, 1.2 $MgSO_4$, 1.2 KH_2PO_4, 10 Hepes, pH 7.4) with/without 10 μM desipramine (DS) before [^{3}H]MPP^+ or ASP^+ exposure to define nonspecific uptake, well above the DS IC_{50}. Between 0.5 and 10 μM there is no significance difference in DS displacement of substrate (data not shown, see Ref. 1). After 5 min, cells were washed 3 times at 4 °C with KRH, and accumulated [^{3}H]MPP^+ was determined by liquid scintillation of 1% (w/v) SDS-solubilized cells; [ASP^+] was determined by liquid chromatography and tandem mass spectrometry (LC/MS/MS). An electrospray (+ESI) LC-MS assay with selected reaction monitoring determined [ASP^+] in hNET-293 cells (incubated in 2 μM ASP^+ for 5 min with/without DS). Cells with ASP^+ were solubilized in 1% SDS and treated with control [D]^3-ASP^+ and acetonitrile. Precipitated proteins were pelleted and discarded. Acetonitrile from the supernatant was evaporated and SDS was removed by polymeric anion exchange trap. High performance liquid chromatography was done on a Zorbax SB-C18, 5 μm, 2.1 × 50-mm column in water:acetonitrile gradient buffered with 10 mM ammonium acetate. Mass spectrometric analysis was performed on a Finnigan TSQ-7000 triple quadrapole mass spectrometer with a standard API-1 electrospray ionization source with a 100-μl inner diameter deactivated fused silica capillary. Nitrogen was used for both sheath and auxiliary gas in the mass spectrometer in the selected reaction monitoring mode, to quantify ASP^+ (mass to charge ratio, *m/z* 239 > 223) with [D]^3-ASP^+ (*m/z* 242 > 226) as an internal standard. No other significant chromatographic peaks were present in cell extracts at the retention time of ASP^+ or internal standard. The lower limit measurement was 150 fm on a column (30 nM in cell extract). Absolute recovery of ASP^+ from cell extracts was greater than 70%. The polymeric strong anion exchange trap reduced SDS content from 1 to ~0.03%. Peak area ratios were evaluated using linear regression weighted with the inverse square of [ASP^+]. Calibration range was 150–5000 fmol on the column (30–1000 nM ASP^+ in original samples). Evaluation of multipoint calibrations in triplicate yielded concentrations of standards within 10% of the theoretical value.

Microscopy—Cells were plated on 35-mm glass-bottom Petri dishes (MatTek, Ashland, MA) coated with poly-L-lysine 3 days before experimentation.

Confocal and Spectra Imaging—Confocal images were taken as described previously (1): culture medium was aspirated and cells immediately mounted on a Zeiss 510 confocal microscope centrally focused on a monolayer using differential interference contrast. Autofluorescence was established from images taken 10 s before adding ASP^+. The argon laser was tuned to 488 nm; emitted light was filtered with a 580-nm lp filter (λ_{max} = 610 nm). ASP^+ accumulation was measured from average pixel intensity of time-resolved fluorescent images in a differential interference contrast-identified region. Average pixel intensity was used to normalize the data. Membrane-localized ASP^+ is defined by a line-scan (3 pixel width) corresponding to a differential interference contrast image. HEK293 cells endogenously accumulate ASP^+ (41); NET-mediated ASP^+ accumulation is defined as hNET-293 minus HEK293 fluorescence. Spectral images were collected using the Meta detector on the Zeiss 510. Emitted light was divided into 10-nm segments ranging from 550 to 700 nm. The average pixel intensity in a region of interest was used to generate an ASP^+ spectrum.

FLIM and Lifetime Spectroscopy—FLIM experiments were performed at the University of Illinois, Champaign-Urbana, in collaboration with N. Barry and E. Gratton (42): hNET-293 cells were exposed to 2 μM ASP^+ for 5 min before imaging, and in 2 μM ASP^+ several intensity and lifetime images were collected. Lifetimes were established by measuring phase and modulation shifts for ASP^+ fluorescence excited by a Ti-sapphire laser at 80 MHz tuned to 920 nm. Calculations for heterdyne frequency measurements are described in Refs. 43–45. The electronic delay was calibrated using 50 nM rhodamine. Lifetime spectroscopy was performed using a Life Spec spectrometer (Edinburgh, Scotland) coupled to a Ti-sapphire laser (Coherent, Santa Clara, CA) producing femtosecond pulses at 1 MHz.

TIRF Microscopy—TIRF images were collected on an Olympus IX-70 with TIRF illumination (Olympus, Melville, NY) and dual-view multiimage acquisition (Optical Insights, Santa Fe, NM) with an Orca ER camera (Hamamstu, Bridgewater, NJ). Channel cross-talk (GFP signal in the ASP^+ window, or *vice versa*) was measured by 10-s images taken before ASP^+ exposure, and no cross-talk occurred.

FCS—Simultaneous GFP-hNET and ASP^+ measurements were taken on a Zeiss 510 with confocal II FCS module. GFP-hNET and ASP^+ were excited with a 488-nm laser, with emitted light separated with 635 nm long pass dichrohic. GFP-hNET and ASP^+ emission were filtered using a 505–530 and 585 band pass. No GFP signal was measured in the ASP^+ channel, or *vice versa*. For all FCS data, the *z*-position was fixed at the cell membrane coverslip face to minimize mitochondrial contributions. If the ASP^+ signal increased over the initial 10-s interval, data were discarded. ASP^+ binding was equilibrated in <1 s (1). We collected fluorescence for 10 s in 15 replicates, with auto- and cross-correlation functions determined for each replicate. The back aperture was overfilled to minimize one-photon FCS artifacts (46), and the focal volume was calibrated using 30 nM rhodamine 6G. FCS measures fluctuations in fluorescence that arise from particle diffusion in the optical volume, chemical reactions, or environmental changes, and the autocorrelation $G(\tau)$ reveals time constants of these processes. Following the formulation in Ref. 46, we used the following equation.

$$G(\tau) = \frac{1}{N}\left(\frac{1 - F_B + F_B e^{-\tau/\tau_B}}{1 - F_B}\right)\left(\sum_{i=1}^{n}\frac{f_i}{(1 + \tau/\tau_{Di})\sqrt{1 + \tau/\omega^2\tau_{Di}}}\right) \quad \text{(Eq. 1)}$$

The fluctuations depend on the number of particles, N, the characteristic diffusion time, τ_{Di}, of those particles in the observation volume, a structure parameter, ω, the weighting factor, f_i, the dark fraction, F_B, and time constant, τ_B, for dark to bright conversion. A detailed discussion of the FCS theory is described in Ref. 47.

Fluorescence Recovery After Photobleach—FRAP measurements were made using a procedure described in Ref. 48: GFP-hNET images were acquired with a ×40 (NA = 1.3) objective (×4 digital zoom) on a Zeiss 510. Three pre-bleach images were acquired before bleaching a 4 × 17.5-μm strip of membrane, and data were fit to an inhomogeneous diffusion model (49).

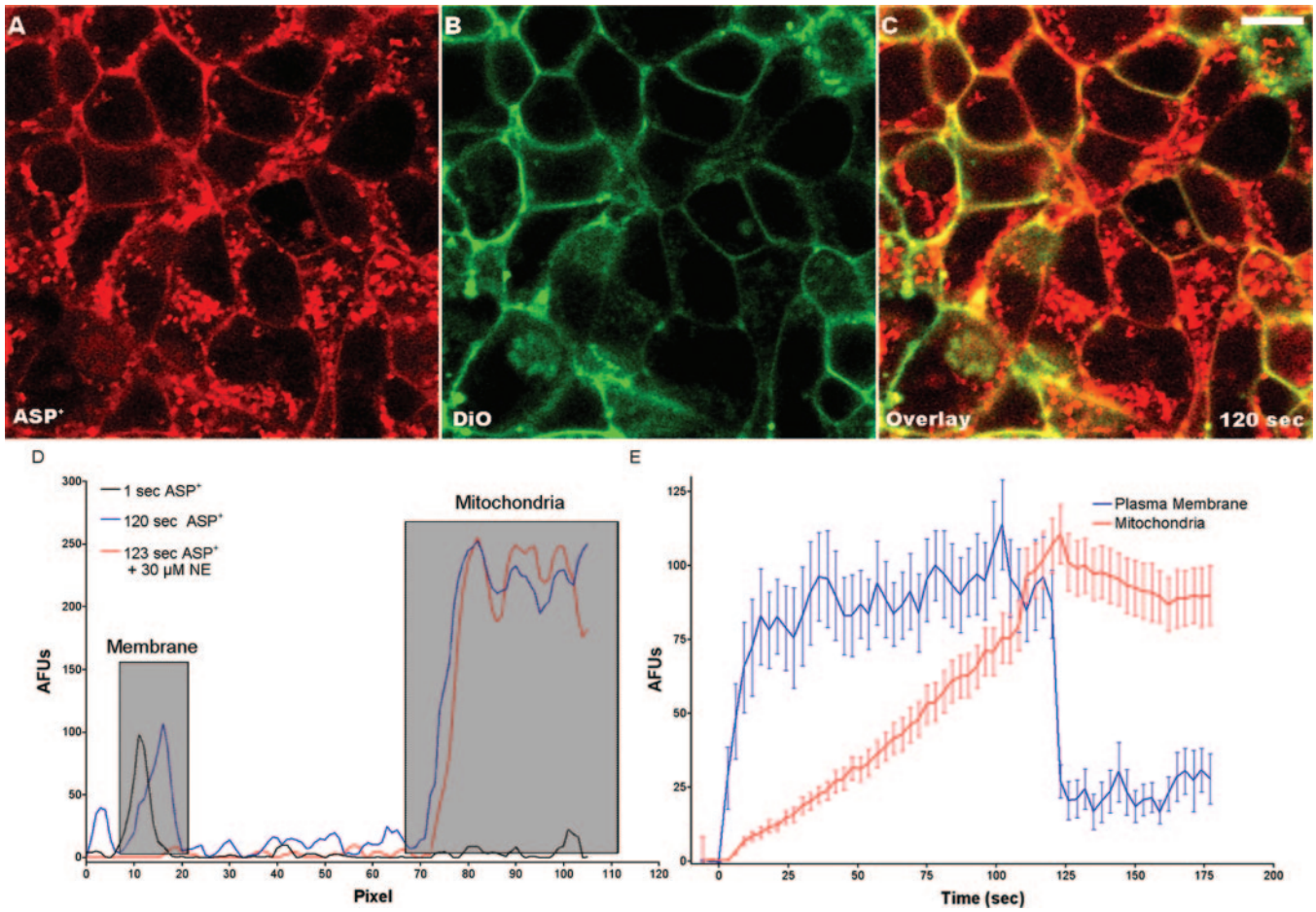

FIG. 1. **ASP$^+$ localizes to the plasma membrane and mitochondria.** *A–C*, hNET-293 cells preincubated with 500 nM DiO for 20 min before 2 μM ASP$^+$ for 2 min: ASP$^+$ fluorescence (*A*), DiO fluorescence (*B*), and co-localization (*C*). *D*, line scan through a hNET-293 cell, from bath through plasma membrane and into mitochondria, examined at 3 s, 120 s (before NE), and 123 s (after 30 μM NE). *E*, temporal fluorescence changes for plasma membrane and mitochondrial ASP$^+$ examined before and after 30 μM NE. NE added 120 s after ASP$^+$ (average ± S.E., n = 150). The *calibration bar* in *panel C* represents 10 μm.

Whole Cell Voltage Clamp—hNET-293 cells on glass coverslips were washed 2 times with bath solution and mounted in a perfusion chamber (SD instruments, San Diego, CA) on an Olympus IX-70 microscope. Whole cell voltage clamp was achieved with an Axopatch 200 B amplifier (Axon instruments, San Diego CA), as described in Ref. 32. Bath solution was (in mM): 130 NaCl, 1.3 KH_2PO_4, 0.5 $MgSO_4$, 1.5 $CaCl_2$, 10 Hepes, 34 glucose, adjusted to pH 7.35 with NaOH and 300 mosmol liter^{-1} with glucose. Pipette solution was (in mM): 120 KCl, 2 $MgCl_2$, 0.1 $CaCl_2$, 1 EGTA, 10 Hepes, 30 glucose, adjusted to pH 7.35 with KOH and 270 mosmol liter^{-1} with glucose. ASP$^+$ or NE were added freshly to the bath solution at 2 and 30 μM, respectively, and perfused with a gravity driven system. All data related to ASP$^+$ solution exchange (except infinite dilution experiments) were taken at 3 s or later, with ASP$^+$ at its full concentration. ASP$^+$ is quenched until bound, further insuring that we monitor only the kinetics of bound and subsequently transported ASP$^+$.

RESULTS

Optical Isolation of Plasma Membrane and Mitochondrial Localized ASP$^+$—To investigate ASP$^+$ bound to plasma membrane-localized NET, we used subcellular organelle stains. hNET-293 cells were stained with 500 nM 3,3′-dioctadecyloxacarbocyanine perchlorate (DiO) for 20 min prior to ASP$^+$ exposure. ASP$^+$ is optically isolated from DiO, a membrane-specific marker (Fig. 1, *A* and *B*). Imaging DiO-stained cells for 10 s before adding ASP$^+$ showed negligible cross-talk between ASP$^+$ and DiO channels. Initially, ASP$^+$ staining co-localizes with DiO fluorescence (first 3 s, data not shown). After 3 s, we observe intracellular punctuated ASP$^+$ distributions (Fig. 1*A*) not co-localized with DiO (Fig. 1*C*). Instead, punctuated intracellular ASP$^+$ co-localizes with a mitochondria stain (MitoTracker Green Molecular Probes, Eugene OR, data not shown), whereas plasma membrane ASP$^+$ is still co-localized with DiO (Fig. 1*C*, yellow). *Panel D* shows the average pixel intensity along a 3-pixel width line from the bath, through the plasma membrane, to the mitochondria. In the first seconds (*black line*), fluorescence localizes to the plasma membrane. After 120 s (*blue*), mitochondrial ASP$^+$ is significant. Subsequent exposure to NE (30 μM) displaces plasma membrane ASP$^+$ without altering mitochondrial fluorescence (Fig. 1*D*, *red*). HEK293 cells measured in parallel demonstrate <0.5% membrane binding and <10% mitochondrial staining. Although line scans separate plasma membrane from deep mitochondria, circumference fluorescence may not report pure plasma membrane. Imperfect separation of near-membrane mitochondria from membrane movement results in ~25% residual fluorescence in the membrane component, because of relatively low spatial resolution of confocal microscopy and cellular movement during the 2-min incubation. With these restrictions, data in Fig. 1*A* are quantified in *panel E*. Plasma membrane-localized fluorescence saturates after ~6 s (*blue*), whereas mitochondrial ASP$^+$ continues to increase (Fig. 1, *red*). At 120 s, 30 μM NE displaces plasma membrane ASP$^+$ and arrests accumulation of mitochondrial ASP$^+$. To improve resolution we use TIRF microscopy (below).

Transporter Plasma Membrane Distribution—TIRF microscopy examines a narrow evanescent field (<1000 Å) where cells

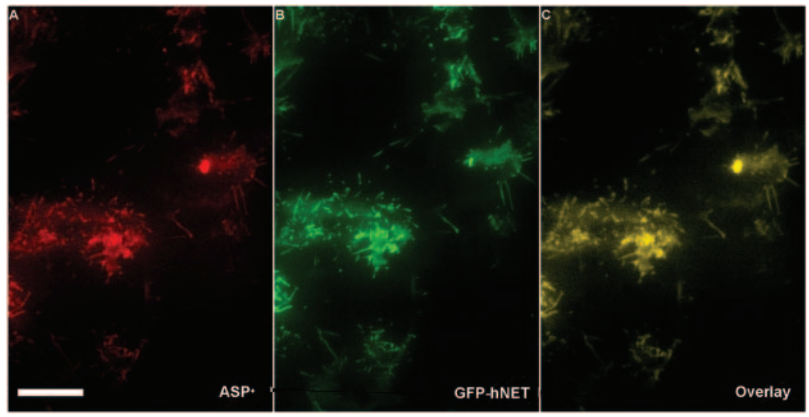

FIG. 2. **GFP-hNET molecules co-localize with ASP$^+$ at the plasma membrane.** Using TIRF microscopy, ASP$^+$ (*A*) and GFP-hNET (*B*) were simultaneously imaged. Images are overlaid in *C*. The *calibration bar* in *A* represents 10 μm.

contact the coverslip (50) (Fig. 2). *Panel A* shows ASP-bound to transporters clustered on the surface and localized to thin filaments at pseudopodia. ASP$^+$ exhibits an identical pattern to GFP-hNET (Fig. 2*B*) and is displaced by 1 μM DS. To evaluate membrane folding as a source of this pattern, we compared DiO HEK293 cells and GFP-hNET-293: only DiO images were uniform, whereas GFP images show patterns. These data demonstrate co-localization of ASP$^+$ and GFP-hNET in the evanescent field (Fig. 2*C*), although the distribution of the paired molecules varies widely. Time-resolved patterns indicate substrate-transporter complexes constantly migrating on the surface, but total surface expression remains constant.

ASP$^+$ and GFP-calibrated Images—To determine the stoichiometry of ASP$^+$ to transporters we used FLIM (see "Materials and Methods"). The fluorescence generated from a population of molecules is dependent on: 1) absorbability (molar extinction); 2) path length; 3) excitation light intensity; 4) quantum yield; and 5) concentration. Knowing this enables conversion of ASP$^+$ fluorescence (AFU) to molecular number (51). Cellular ASP$^+$ fluorescence lifetime was determined by fluorescent phase shift and modulation using heterodyne frequency domain measurements (43, 45). To determine the cellular ASP$^+$ fluorescence lifetime, hNET-293 cells were exposed to 2 μM ASP$^+$ for 5 min. The intensity image (Fig. 2*A*) shows that ASP$^+$ binding is strongest along the plasma membrane, but the signal also arises from mitochondrial regions inside the cell. Using the intensity image as a template, the lifetime of ASP$^+$ can be determined from FLIM (Fig. 2*B*) on the plasma membrane and in the mitochondria. The heterdyne frequency method provides two measurements of the average lifetime in a diverse population, τ_{phase} and τ_{mod}. The former measures lifetime via changes in phase of the excitation fluorescence, the latter measures changes in frequency modulation of the excitation fluorescence. Average ASP$^+$ lifetimes were equal for plasma membrane and mitochondrial fluorescence (τ_{phase} and τ_{mod} were 2.5 $\pm$ 0.5 and 1.8 $\pm$ 0.36 ns, respectively), indicating that an increase in ASP$^+$ quantum yield is statistically identical whether bound to hNET or localized in mitochondria. The mitochondria binding target is unknown; however, FLIM data show that all cellular fluorescence (mitochondria or plasma membrane) can be converted to absolute numbers of ASP$^+$ molecules using the same conversion factor. Because FLIM showed no heterogeneity of ASP$^+$ lifetimes, further calibrations were done in cuvettes on a lifetime spectrometer. To find a suitable calibration solution we investigated isobutyl alcohol acetone, 1-propanol, isopropyl alcohol, Me_2SO (dimethyl sulfoxide), chloroform, acetone, and tetrahydrofuran. None of these solvents altered ASP$^+$ absorbtion spectra (data not shown), but they had marked effects on emission spectra. ASP$^+$ emission spectra in isobutyl alcohol, 1-propanol, and isopropyl alcohol were similar to that from cellular ASP$^+$, but the Me_2SO spectrum shifted and was less fluorescent (Fig. 3*C*). Plasma membrane ASP$^+$ had identical spectra to mitochondrial ASP$^+$. ASP$^+$ in isobutyl alcohol generates the highest quantum efficiency of the solvents tested and is a spectral match for cellular ASP$^+$, thus we used it as the calibration solvent. hNET-293 cells were incubated with 2 μM ASP$^+$ for 5 min prior to harvest. Cells were suspended in KRH ("Materials and Methods"), and cellular lifetime data were compared with ASP$^+$ in isobutyl alcohol (Fig. 3*D*), which revealed one lifetime. Cellular ASP$^+$ signals consist of several species with different lifetimes indicated by multiexponential decay (Fig. 3*D*). The weighted average of these lifetimes were used for calibration. To control for data acquisition parameters, identical microscope conditions were used for cellular and calibration ASP$^+$ fluorescence. The confocal pinhole, laser intensity, and z-axial positions were also identical, controlling for differences in optical volumes defined by the confocal point spread function. Measuring lifetimes in cells and the calibration solvent controlled for differences in quantum yield, defined as photons emitted divided by photons absorbed. Quantum yield also equals fluorescence lifetime divided by intrinsic lifetime (51). Although intrinsic lifetime is unknown, it is constant for each molecule; thus, the change in quantum yield in cellular *versus* calibration equals the ratio of fluorescence lifetimes (Fig. 3*D*). In isobutyl alcohol, ASP$^+$ has an average lifetime of 168 ps, compared with 1200 ps for cellular ASP$^+$. A factor of seven converts cellular fluorescence to ASP$^+$ concentration. Fig. 3*E* shows calibrations for ASP$^+$ and GFP. Confocal images of ASP$^+$ in isobutyl alcohol and GFP in aqueous buffer were acquired, and the pixel histogram peak was plotted against concentration. GFP fluorescence is relatively independent of the local environment; thus lifetime corrections similar to ASP$^+$ were not required (52). Calibrations were performed daily and all experiments below were performed using calibrated conditions.

Transporter/Substrate Ratios—GFP-hNET accumulation for NE and ASP$^+$ was identical to hNET, and GFP-hNET and hNET demonstrate no difference in ASP$^+$ binding (data not shown). We collected ASP$^+$ and GFP-hNET data using calibrated settings (Fig. 3) and converted pixel intensity to molecular values. Fig. 4*A* shows an overlay image 10 s after applying ASP$^+$; the yellow color at cell borders signifies GFP-hNET and ASP$^+$ co-localization, whose ratio was calculated by dividing GFP-hNET images by ASP$^+$ images at each time. Fig. 4*B* shows the ratio at 10 s. Inside the cell, the co-localization ratio approaches zero. Furthermore, although the GFP-hNET/ASP$^+$ ratio intensity varies along the cell perimeter (Fig. 4*A*), the value is approximately constant (numerical value represented by color, Fig. 4*B*) and time independent (Fig. 4*C*). *Panel D* quantifies the ratio from the maximum GFP-hNET and ASP$^+$ molecules along a four-pixel wide line scan along the cell circumference. Data are summed over time for each cell (n = 250),

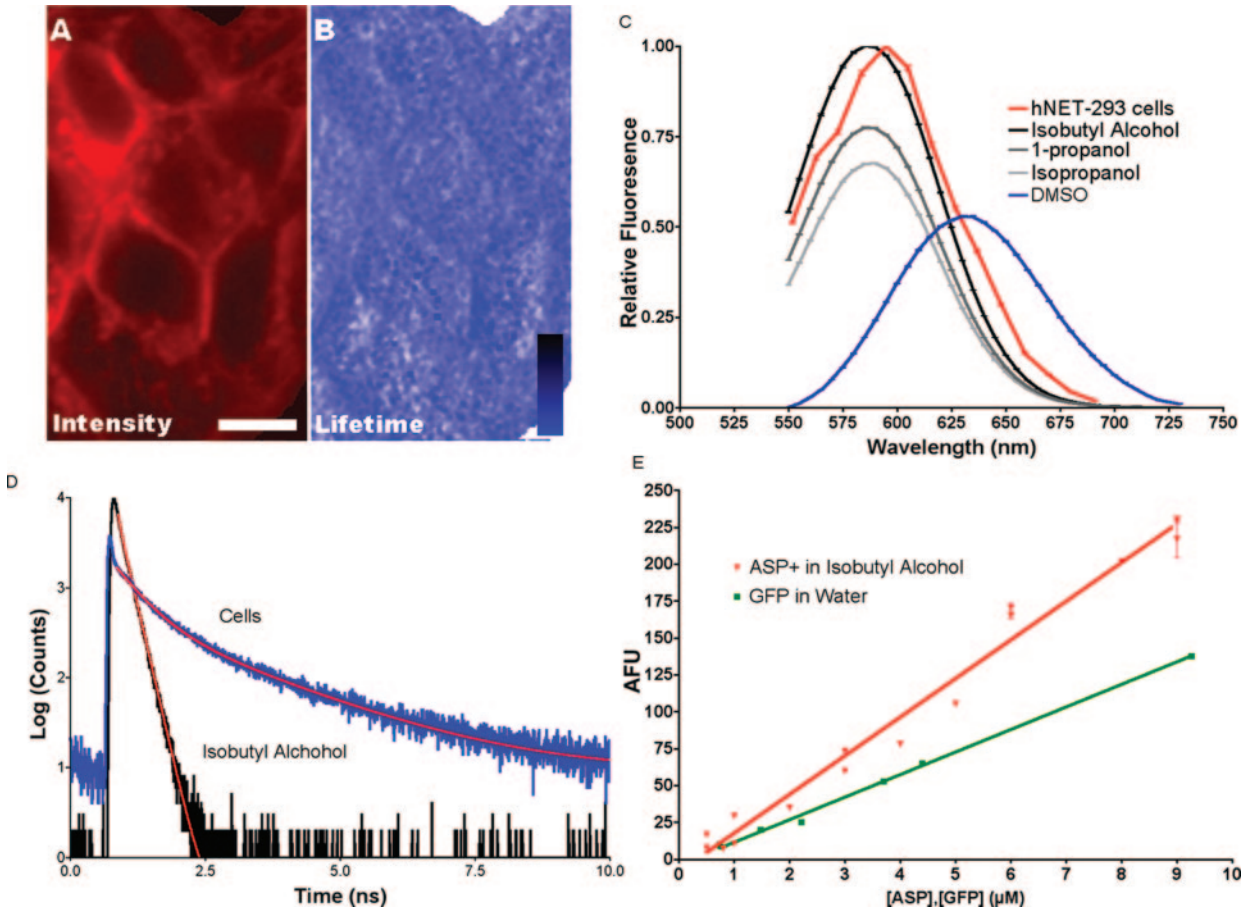

FIG. 3. **ASP$^+$ and GFP quantification.** *A* and *B*, hNET-293 cells were exposed to 2 μM ASP$^+$ for 5 min prior to image acquisition. Changes in fluorescence intensity (*A*) and fluorescence lifetime (*B*) were examined using FLIM (see "Materials and Methods"). The color gradient in *B* indicates fluorescence lifetime, with *black* as the longest lifetime. *C*, emission spectra for several solvents and cellular ASP$^+$ assessed using an L-format spectrometer and spectral imaging, respectively (Zeiss 510, Meta) (average ± S.E., $n = 3$). The solvent spectra, isobutyl alcohol, 1-proponal, isopropyl alcohol, and Me_2SO normalized to ASP$^+$ (2 μM) maximum in isobutyl alcohol; hNET-293 spectrum was normalized to λ_{max}. Mitochondria and membrane fluorescence have identical emission spectra. *D*, cellular ASP$^+$ lifetime quantified using time-resolved fluorescence spectroscopy. ASP$^+$ lifetime in the calibration solvent, isobutyl alcohol, and cell was measured in a lifetime spectrometer. Cellular lifetime was measured by preloading hNET-293 cells with 5 μM ASP$^+$ for 10 min prior to harvest and washing. Log photon-count is plotted against time and the data are fit to multiexponential function (counts $= A + Be^{-t/\tau} + Ce^{-t/\tau} + De^{-t/\tau} \ldots$). *E*, identical imaging settings, increasing concentrations of ASP$^+$ in isobutyl alcohol, and GFP in water were imaged. The average pixel intensity across an image plane of 10 μm from the coverslip was plotted against concentration (average ± S.E., $n = 3$, ASP$^+$ slope = 26.5 AFU/μM, $r^2 = 0.980$, GFP slope = 15.3 ± 0.41 AFU/μM, $r^2 = 0.997$). The *calibration bar* in *panel A* represents 10 μm.

and the peak represents the expected value. Thus one GFP-hNET molecule binds to one ASP$^+$ molecule; that is, one substrate associates with each hNET protein.

ASP$^+$ Residence Time and Transporter Number—FCS (see "Materials and Methods") yields information about molecular concentration, kinetics, and mobility (53). We used dual-channel FCS to simultaneously measure GFP-hNET and ASP$^+$ fluctuations before and after 2 μM ASP$^+$ exposure (Fig. 5). Bath ASP$^+$ demonstrates diminished fluorescence ($\tau_{water} < 10$ ps) compared with cellular ASP$^+$ ($\tau_{cells} = 1.2$ ns), which permits the identification of bound *versus* free ASP$^+$. Nonspecific staining is less than 0.5% of the total signal (1). The autocorrelation function of ASP$^+$ intensity fluctuations, $G(\tau)$, reveals an ASP$^+$ transporter residence time of 526 ± 25 μs (Fig. 5), significantly different from the relaxation for GFP-hNET measured in the same optical volume (~0.15 fL, "Materials and Methods"). Preincubation with 1 μM DS disrupts the ASP$^+$ autocorrelation function without altering the GFP-hNET autocorrelation function. FCS experimentation is sensitive to reactions between 10 μs to 100 ms (54). If ASP$^+$ dissociation were greater than 100 ms, $G(\tau)$ for ASP$^+$ and GFP would be virtually identical. We did not observe cross-correlation between ASP$^+$ and GFP. ASP$^+$ K_D is 460 ± 60 nM (1), which we correlated with infinite dilution data to measure ASP$^+$ dissociation. hNET-293 cells were exposed to 2 μM ASP$^+$ for 30 s before 4 ml of KRH, and the [ASP$^+$] was diluted to 10 nM (1:200). These data yielded an off rate (k^-) for ASP$^+$ of 0.43 ± 0.009 s^{-1}; the corresponding k^+ is thus 10^6 M^{-1} s^{-1} assuming K_D close to measured IC_{50} (K_m) values (1). Analysis of GFP-tagged transporters gave a relaxation of 30.2 ± 0.94 ms (hNET-GFP diffusion constant (D) = 0.17 μm^2/s, Fig. 5), consistent with slow diffusion of a membrane protein (55, 56). FRAP gave a similar GFP-hNET diffusion time ($D = 0.11 \pm 0.02$ μm^2/s, data not shown). We also observe a 320-μs relaxation, which correlates to pH-dependent interconversion for GFP (57). The $\tau = 0$ intercept ($1/N$) gives an average transporter number (53) of $N_{ASP+} = 26.8 \pm 1.07$ (bound) ASP$^+$ particles and $N_{GFP} = 26.3 \pm 1.2$ GFP-hNET particles in the optical volume, which agrees with the FLIM data (Fig. 4). At 2 μM, 0.15 fL contains 180 total ASP$^+$ molecules, of which 26 are bound and fluoresce. From these data we estimate ~4.8×10^5 ASP$^+$ and GFP molecules/cell, similar to hNET surface expression by calibrated confocal, and to radiolabeled antagonist binding estimates (32).

Surface Density and Transport Velocity—The FCS data correlate to three processes, ASP$^+$ association, ASP$^+$ disassociation, and ASP$^+$ transport. We also measured total ASP$^+$ influx

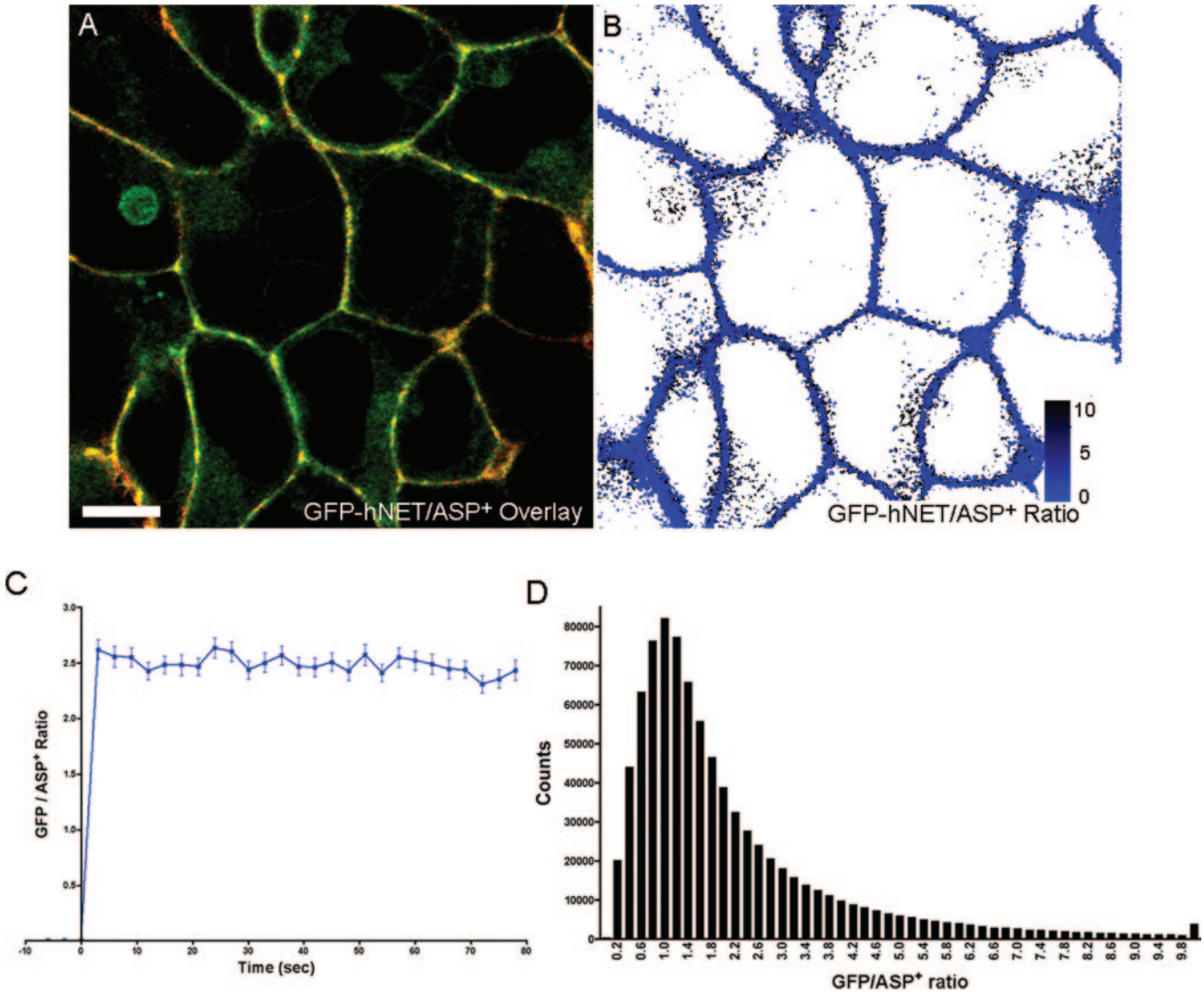

FIG. 4. **GFP-hNET/ASP$^+$ ratio is constant.** *A*, GFP-hNET-293 cells were exposed to 2 μM ASP$^+$ and the number of GFP-hNET and ASP$^+$ molecules within each pixel was determined by quantitative imaging. ASP$^+$ and GFP-hNET values are represented by *red* and *green* intensities, respectively. The overlay image demonstrates the relative color contributions for each molecule. *B*, the GFP-hNET to ASP$^+$ ratio calculated for pixels that co-localize in the 10-s image. The color gradient in *B* indicates GFP-hNET/ASP$^+$ ratios corresponding to values on the *right*. *C*, average GFP-hNET/ASP$^+$ ratio determined for each image after ASP$^+$ (2 μM) (average ± S.E., n = 15). *D*, GFP-hNET/ASP$^+$ ratio determined for each pixel within a 4-pixel width line scan around the circumference of GFP-hNET cells. The histogram represents all pixel values across these line scans for all cells over several experiments (n = 250 cells). The *calibration bar* in *panel A* represents 10 μm.

after the addition of ASP$^+$. Three-dimensional, single-cell *z*-series were collected seven times, 30-s per point, and Fig. 6 shows total ASP$^+$ (surface and interior) in the stack. The break in Fig. 6*A* represents bound ASP$^+$, and the slope of the 2nd phase is uptake velocity (1), which depends on surface transporter number, and turnover rate is velocity/number. Fig. 6*B* shows this ratio for cells with low and high expression. At 21 °C, turnover is 0.012 ± 0.0011 ASP/hNET-protein/s, whereas MPP$^+$ (by radiometry) is 0.116 ± 0.012 MPP/hNET-protein/s); at 34 °C ASP$^+$ turnover is 0.024 ± 0.0018 ASP/hNET-protein/s, thus Q_{10} = 2.1. Because these data include only ASP$^+$ bound to mitochondria, we also measured total accumulation by LC/MS/MS (liquid chromatography and tandem mass spectrometry, see "Materials and Methods"), yielding 0.055 ± 0.012 ASP/hNET-protein/s). In LLC-PK1 cells, NE turnover is 0.05 NE/s/transporter at room temperature (31). At 37 °C, COS cells have a 2NE:MPP V_{max} ratio, and MPP$^+$ turnover of 0.65 MPP/hNET-protein/s (58). The Q_{10} for NET-mediated ASP$^+$ transport is 2.5 (59), and we measured 2.1 (data not shown). Thus at 21 °C, MPP$^+$ turnover would be 0.2 MPP/hNET-protein/s.

DISCUSSION

To measure substrate-transporter stoichiometry requires quantitative separation of plasma membrane-bound substrate from the transported substrate. These pools are easily distinguished using the fluorescent substrate, ASP$^+$. Externally applied NE displaces plasma membrane-bound ASP$^+$, but not mitochondrial-bound (transported) ASP$^+$. Furthermore, ASP$^+$ localization to cell compartments does not alter its fluorescence; thus, the same calibration factor applies throughout the cell (Fig. 3). Calibrated ASP$^+$ and GFP-hNET images yield a 1:1 substrate:hNET ratio (Fig. 4). ASP$^+$ is optically silent unless bound to hNETs or to mitochondria; however, because GFP-hNET is not exclusively localized to the plasma membrane, FLIM-calibrated stoichiometry measurements may be an underestimate. To improve spatial resolution, we used TIRF imaging, which restricts data collection to ~100 nm at the cell

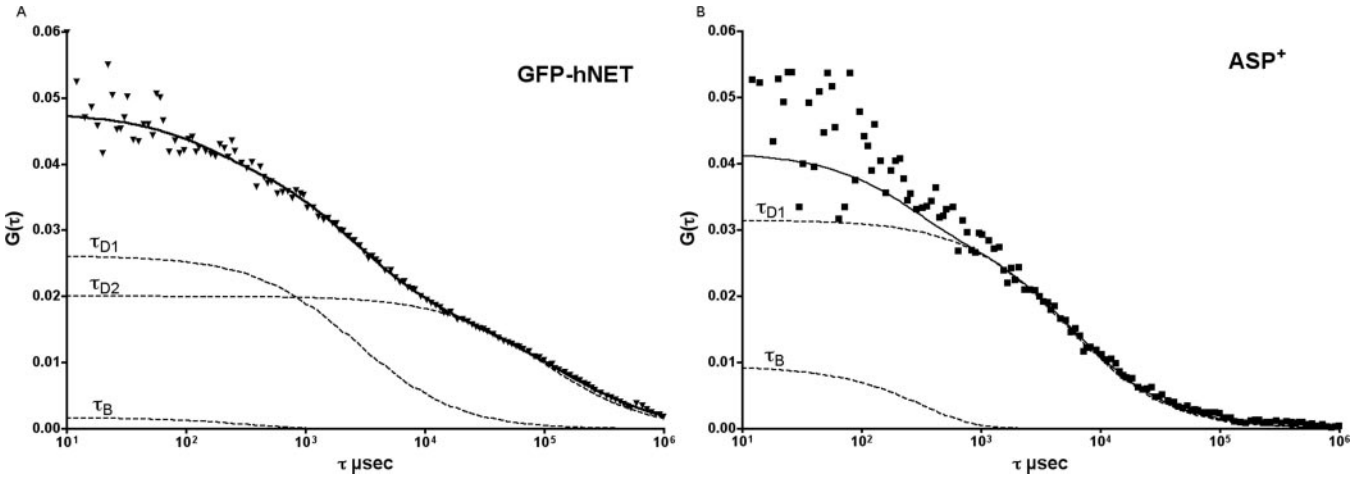

FIG. 5. **ASP$^+$ associates with GFP-hNET for 526 μs.** *A*, GFP-hNET-293 cells were exposed (*B*) to 2 μM ASP$^+$, and fluorescence fluctuations were fit to the autocorrelation function G(τ) (Equation 1) (n = 15 cells with 10 replicates). *Dashed lines* represent relative contributions of individual fit parameters to the entire autocorrelation function. τ_{D1} and τ_{D2} represent fits for individual diffusion times, and τ_B represents the contribution of the triplet state. The fits yield the following parameters: N_{ASP+} = 26.8 ± 1.07, N_{GFP} = 26.3 ± 1.2, $\tau_{D1(ASP+)}$ = 526 ± 25 μs, $\tau_{D1(GFP)}$ = 320 ± 15 μs, $\tau_{D2(GFP)}$ = 30.247 ± 2.4 ms, $\tau_{B(ASP+)}$ = 34.4 ± 3.3 μs, and $\tau_{B(GFP)}$ = 29.7 ± 2.9 μs.

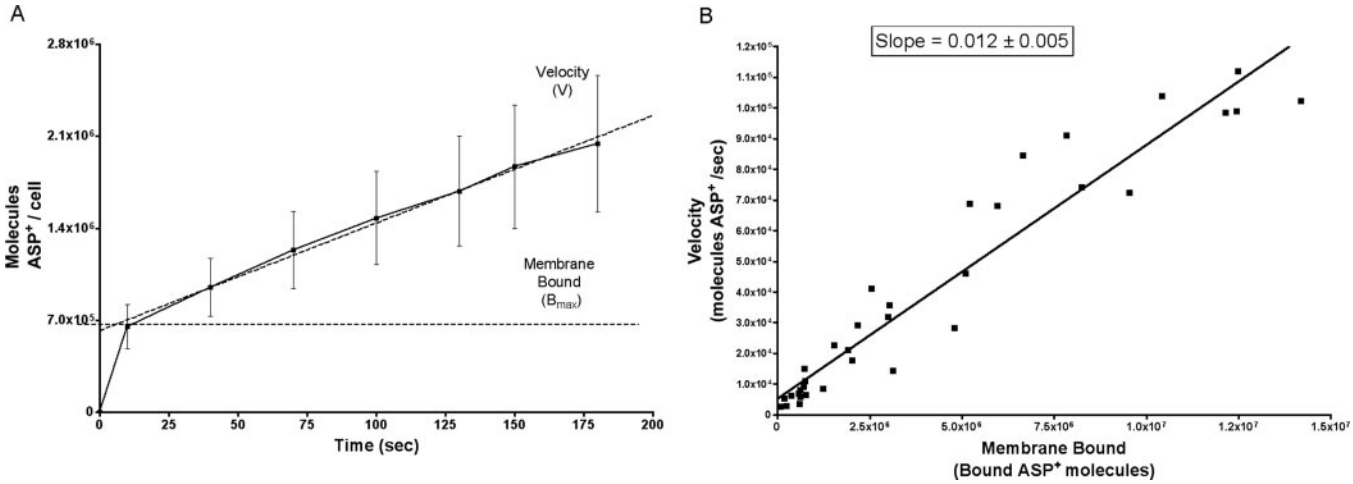

FIG. 6. **hNET-mediated ASP$^+$ transport.** A, *z*-series encompassing single hNET-293 cells exposed to 2 μM ASP$^+$ were sampled in 30-s intervals for 4 min. Total number of ASP$^+$ molecules determined at each time (average ± S.E., n = 15) (bound = 623,000 ± 8,270 molecules/cell, velocity = 8,180 ± 73.0 molecules/cell, average ± S.E.). *B*, bound ASP$^+$ molecules compared with velocity of ASP$^+$ molecules accumulating inside cell clusters (1–5 cells). Bound state as assessed by initial fluorescence increase, and velocity were established by the change in total molecules. Dividing velocity by the number of bound transporters is the transport rate (0.012 ± 0.005, average ± S.E., n = 35, r^2 = 0.93).

surface (Fig. 2). TIRF time series show that surface hNET is mobile, but the number is constant, and, at near saturating [ASP$^+$], most surface hNETs are occupied. Because ASP$^+$ and GFP-hNET numbers are equivalent (Fig. 5), GFP-hNET near the inner face of the membrane contributes insignificantly, confirming a 1:1 substrate:hNET protein stoichiometry. Thus, if hNET were a tetramer, four substrate molecules would bind to each functional transporter. Recent structural studies indicate that in a glutamate transporter, the subunit binds one substrate (60, 61).

The GFP-hNET membrane diffusion time constant of 30 ms is slow compared with the ASP$^+$ dwell time of 526 μs (Fig. 5), the latter representing the light-generating reaction in which ASP$^+$ goes from the bound quenched state to the bound bright state, B $\Leftarrow$ B*. ASP$^+$ fluorescence quenching most likely occurs via hydration with water upon dissociating from the transporter, and not by pH modulation, interaction with co-transported ions, protein conformational movements, or energy transfer to hNET. ASP$^+$ fluoresces in aqueous solutions with a pH ranging from 2 to 11, so ASP$^+$ fluoresces under physiological conditions. Furthermore, neither Na^+ nor Cl^- quench ASP$^+$ in solution, and local Na^+ or Cl^- interactions should not affect fluorescence. For protein movement to quench ASP$^+$, hNET would adopt a conformation permitting ASP$^+$ rotation, but anisotropy data show that bound ASP$^+$ is in a rigid position (1). Energy transfer from ASP$^+$ to NET is unlikely because no amino acids share significant spectral overlap with ASP$^+$ emission. ASP$^+$ quantum efficiency changes after binding is likely attributed to rigidly bound ASP$^+$, thus the rapid relaxation we observe is likely attributed to ASP$^+$ release into an aqueous environment. Rapid ASP$^+$ quenching is most probably ASP$^+$ release into a local water-filled cavity, and the dark-to-bright kinetics likely represent a restricted reaction, similar to the ternary model for G-protein-coupled receptors (62, 63), or the isomerization model for ligand-gated ion channels (64).

At steady state and −100 mV, ASP$^+$ generates 4 pA through hNET, whereas NE generates >20 pA under the same conditions. Fifty ms after adding ASP$^+$, ~700 elementary charges move per transported ASP$^+$, but only ~50 charges move per NE (65). Thus ASP$^+$ generates less current than NE, but more net relative charge. The infinite dilution dissociation rate of 430 ms describes the average time ASP$^+$ associates with hNET. This is distinct from the FCS rate of 526 μs, interpreted as local ASP$^+$ isomerizations ~2000 times/s. ASP$^+$ is effec-

tively sequestered by hNET and only released from a binding pocket ~2 times/s. For each transport event, 36,000 isomerizations occur and 36 molecules escape, resulting in a turnover of 0.06/s. These data could be different *in vivo*, but we propose that slow transport may reflect incompetent binding rather than large conformational changes of the protein.

Acknowledgments—Imaging analyses were performed in the VUMC Cell Imaging Core Resource under S. Wells. We thank P. Bissel and N. Castagnoli for the synthesis of $[D]^3$-ASP^+, N. Barry and E. Gratton of the Laboratory for Fluorescence Dynamics, University of Illinois, for assistance with the FLIM studies, and M. L. Mainer for the LC/MS/MS ASP^+ assay. We also thank R. Blakely for thought provoking discussions and A. Kenworthy for assistance with FRAP and FCS. We especially thank Hongping Yuan for technical assistance.

REFERENCES

1. Schwartz, J. W., Blakely, R. D., and DeFelice, L. J. (2003) *J. Biol. Chem.* **278,** 9768–9777
2. Valentino, R. J., Foote, S. L., and Aston-Jones, G. (1983) *Brain Res.* **270,** 363–367
3. Trendelenburg, A. U., Gaiser, E. G., Cox, S. L., Meyer, A., and Starke, K. (1999) *J. Neurochem.* **73,** 1431–1438
4. Foote, S., and Aston-Jones, G. (1995) *Pharmacology and Physiology of Central Noradrenergic Systems. Psychopharmacology: The Fourth Generation of Progress*, Raven Press Ltd., New York
5. Schildkraut, J. J., Gordon, E. K., and Durell, J. (1965) *J. Psychiatr. Res.* **3,** 213–228
6. Clark, M. S., and Russo, A. F. (1998) *Brain Res. Brain Res. Protoc.* **2,** 273–285
7. Maes, M., Lin, A. H., Verkerk, R., Delmeire, L., Van Gastel, A., Van der Planken, M., and Scharpe, S. (1999) *Neuropsychopharmacology* **20,** 188–197
8. Backs, J., Haunstetter, A., Gerber, S. H., Metz, J., Borst, M. M., Strasser, R. H., Kubler, W., and Haass, M. (2001) *J. Mol. Cell Cardiol.* **33,** 461–472
9. Axelrod, J., and Kopin, I. J. (1969) *Prog. Brain Res.* **31,** 21–32
10. Blakely, R. D. (2001) *J. Neurosci.* **21,** 8319–8323
11. Garland, E. M., Hahn, M. K., Ketch, T. P., Keller, N. R., Kim, C. H., Kim, K. S., Biaggioni, I., Shannon, J. R., Blakely, R. D., and Robertson, D. (2002) *Ann. N. Y. Acad. Sci.* **971,** 506–514
12. Robertson, D., Flattem, N., Tellioglu, T., Carson, R., Garland, E., Shannon, J. R., Jordan, J., Jacob, G., Blakely, R. D., and Biaggioni, I. (2001) *Ann. N. Y. Acad. Sci.* **940,** 527–543
13. Shannon, J. R., Flattem, N. L., Jordan, J., Jacob, G., Black, B. K., Biaggioni, I., Blakely, R. D., and Robertson, D. (2000) *N. Engl. J. Med.* **342,** 541–549
14. Pacholczyk, T., Blakely, R. D., and Amara, S. G. (1991) *Nature* **350,** 350–354
15. Sacchetti, G., Bernini, M., Bianchetti, A., Parini, S., Invernizzi, R. W., and Samanin, R. (1999) *Br. J. Pharmacol.* **128,** 1332–1338
16. Javitch, J. A., D'Amato, R. J., Strittmatter, S. M., and Snyder, S. H. (1985) *Proc. Natl. Acad. Sci. U. S. A.* **82,** 2173–2177
17. Savchenko, V., Sung, U., and Blakely, R. D. (2003) *Mol. Cell Neurosci.* **24,** 1131–1150
18. Hahn, M. K., Robertson, D., and Blakely, R. D. (2003) *J. Neurosci.* **23,** 4470–4478
19. Kocabas, A. M., Rudnick, G., and Kilic, F. (2003) *J. Neurochem.* **85,** 1513–1520
20. Kilic, F., and Rudnick, G. (2000) *Proc. Natl. Acad. Sci. U. S. A.* **97,** 3106–3111
21. Ramsey, I. S., and DeFelice, L. J. (2002) *J. Biol. Chem.* **277,** 14475–14482
22. Schmid, J. A., Scholze, P., Kudlacek, O., Freissmuth, M., Singer, E. A., and Sitte, H. H. (2001) *J. Biol. Chem.* **276,** 3805–3810
23. Hastrup, H., Sen, N., and Javitch, J. A. (2003) *J. Biol. Chem.* **278,** 45045–45048
24. Hastrup, H., Karlin, A., and Javitch, J. A. (2001) *Proc. Natl. Acad. Sci. U. S. A.* **98,** 10055–10060
25. Norgaard-Nielsen, K., Norregaard, L., Hastrup, H., Javitch, J. A., and Gether, U. (2002) *FEBS Lett.* **524,** 87–91
26. Torres, G. E., Carneiro, A., Seamans, K., Fiorentini, C., Sweeney, A., Yao, W. D., and Caron, M. G. (2003) *J. Biol. Chem.* **278,** 2731–2739
27. Sitte, H. H., Farhan, H., and Javitch, J. A. (2004) *Mol. Intervent.* **4,** 38–47
28. Bonisch, H., Fuchs, G., and Graefe, K. H. (1986) *Naunyn-Schmiedebergs Arch. Pharmacol.* **332,** 131–134
29. DeFelice, L. J. (2004) *Trends Neurosci.* **27,** 352–359
30. Friedrich, U., and Bonisch, H. (1986) *Naunyn-Schmiedebergs Arch. Pharmacol.* **333,** 246–252
31. Gu, H. H., Wall, S., and Rudnick, G. (1996) *J. Biol. Chem.* **271,** 6911–6916
32. Galli, A., DeFelice, L. J., Duke, B. J., Moore, K. R., and Blakely, R. D. (1995) *J. Exp. Biol.* **198,** 2197–2212
33. Larsson, H. P., Picaud, S. A., Werblin, F. S., and Lecar, H. (1996) *Biophys. J.* **70,** 733–742
34. Bruns, D., Engert, F., and Lux, H. D. (1993) *Neuron* **10,** 559–572
35. Bruns, D. (1998) *Methods Enzymol.* **296,** 593–607
36. Jayanthi, L. D., Vargas, G., and DeFelice, L. J. (2002) *Br. J. Pharmacol.* **135,** 1927–1934
37. Ingram, S. L., Prasad, B. M., and Amara, S. G. (2002) *Nat. Neurosci.* **5,** 971–978
38. Carvelli, L., McDonald, P. W., Blakely, R. D., and Defelice, L. J. (2004) *Proc. Natl. Acad. Sci. U. S. A.* **101,** 16046–16051
39. Rudnick, G. (1998) *Methods Enzymol.* **296,** 233–247
40. Ramamoorthy, S., Giovanetti, E., Qian, Y., and Blakely, R. D. (1998) *J. Biol. Chem.* **273,** 2458–2466
41. Stachon, A., Schlatter, E., and Hohage, H. (1996) *Cell. Physiol. Biochem.* **6,** 72–91
42. Hanson, K. M., Behne, M. J., Barry, N. P., Mauro, T. M., Gratton, E., and Clegg, R. M. (2002) *Biophys. J.* **83,** 1682–1690
43. Jameson, D. M., Gratton, E., and Hall, R. D. (1984) *Appl. Spectrosc. Rev.* **20,** 55–106
44. Gratton, E., Jameson, D. M., and Hall, R. D. (1984) *Annu. Rev. Biophys. Bioeng.* **13,** 105–124
45. Alcala, J. R., Gratton, E., and Jameson, D. M. (1985) *Anal. Instr.* **14,** 225–250
46. Hess, S. T., and Webb, W. W. (2002) *Biophys. J.* **83,** 2300–2317
47. Bacia, K., and Schwille, P. (2003) *Methods* **29,** 74–85
48. Cole, N. B., Smith, C. L., Sciaky, N., Terasaki, M., Edidin, M., and Lippincott-Schwartz, J. (1996) *Science* **273,** 797–801
49. Siggia, E. D., Lippincott-Schwartz, J., and Bekiranov, S. (2000) *Biophys. J.* **79,** 1761–1770
50. Axelrod, D. (2001) *Traffic* **2,** 764–774
51. Lakowicz, J. (1999) *Principles of Fluoresence Spectroscopy*, 2nd Ed., Kluwer Academic/Plenum Publishers, New York
52. Patterson, G. H., Knobel, S. M., Sharif, W. D., Kain, S. R., and Piston, D. W. (1997) *Biophys. J.* **73,** 2782–2790
53. Schwille, P. (2001) *Cell Biochem. Biophys.* **34,** 383–408
54. Schwille, P., Haupts, U., Maiti, S., and Webb, W. W. (1999) *Biophys. J.* **77,** 2251–2265
55. Meissner, O., and Haberlein, H. (2003) *Biochemistry* **42,** 1667–1672
56. Vrljic, M., Nishimura, S. Y., Brasselet, S., Moerner, W. E., and McConnell, H. M. (2002) *Biophys. J.* **83,** 2681–2692
57. Haupts, U., Maiti, S., Schwille, P., and Webb, W. W. (1998) *Proc. Natl. Acad. Sci. U. S. A.* **95,** 13573–13578
58. Pifl, C., Hornykiewicz, O., Giros, B., and Caron, M. G. (1996) *J. Pharmacol. Exp. Ther.* **277,** 1437–1443
59. Mason, J. N., Farmer, H., Tomlison, I. D., Schwartz, J. W., Savchenko, V., DeFelice, L. J., Rosenthal, S. J., and Blakely, R. D. (2004) *J. Neurosci. Methods*, in press
60. Yernool, D., Boudker, O., Jin, Y., and Gouaux, E. (2004) *Nature* **431,** 811–818
61. Yernool, D., Boudker, O., Folta-Stogniew, E., and Gouaux, E. (2003) *Biochemistry* **42,** 12981–12988
62. De Lean, A., Stadel, J. M., and Lefkowitz, R. J. (1980) *J. Biol. Chem.* **255,** 7108–7117
63. Samama, P., Cotecchia, S., Costa, T., and Lefkowitz, R. J. (1993) *J. Biol. Chem.* **268,** 4625–4636
64. Del Castillo, J., and Katz, B. (1957) *Proc. R. Soc.* **146,** 369–381
65. Galli, A., Blakely, R. D., and DeFelice, L. J. (1996) *Proc. Natl. Acad. Sci. U. S. A.* **93,** 8671–8676

Substrate Binding Stoichiometry and Kinetics of the Norepinephrine Transporter

Joel W. Schwartz, Gaia Novarino, David W. Piston and Louis J. DeFelice

J. Biol. Chem. 2005, 280:19177-19184.
doi: 10.1074/jbc.M412923200 originally published online March 9, 2005
